Design and Fabrication of a Flapping-Wing Robot Based on Slider-Crank Mechanism

Jue Wang
Milton Academy, USA,
Email: juewang40@gmail.com

Abstract: **Tailless Flapping-Wing Micro Air Vehicles (FW-MAVs) have gained more attention recently because they utilize energy more efficiently compared to fixed-wing aircraft and rotorcrafts. FW-MAVs could be used commercially to explore confined spaces with insufficient air or serve as surveillance robots. However, due to their use of unsteady aerodynamics and small size, the research and design process is very complicated. In this paper, I propose a flight mechanism for a light-weighted, two-winged, hummingbird-inspired flapping-wing robot. Five versions of the robot were built; each version improved upon the issues of the previous one. Calculations were performed to optimize the stroke amplitude and the transmission ratio of the gears. Four groups of control experiments were conducted to investigate the relationship between different factors (voltage, motor type, wing area, and the number of veins) and the robot's lift, which was monitored by a pressure sensor. I analyzed the results from the experiments and built a final version of the robot based on a slider-crank mechanism. The main structure of the final version is made of three 3mm carbon fiber boards, and the wings are made of 0.025mm PET (polyethylene terephthalate) material, reinforced by three carbon fiber rods: two 0.5mm ones across the membrane and a 1mm one at the leading edge. The robot weighs 16.3g and can produce enough lift to overcome its gravity under 9V with an off-board power source by exhibiting an upward trend during a tethered flight test.**

Keywords: **Biomimetics, Flapping-wing, Hummingbird, Slider-Crank**

I. INTRODUCTION

The smallest birds in the world, hummingbirds, can hover in the air by flapping their deformable wings, allowing them to perform agile maneuvers. This flying method has many different advantages that current existing Unmanned Aerial Vehicles (UAV) do not possess. It is very energy efficient even though its wingbeat frequency is very high [1]. The wings are usually light, resulting in smaller wing inertia, thus less energy would be consumed to activate the wings. Compared to fixed-wing aircraft, which consume a lot of energy because they convert air resistance into lift through the airfoil (Bernoulli's Theorem) and the angle of attack (AOA), FW-MAVs use most of their energy to flap their wings, directly producing lift [2]. Flapping-wing robots generate thrust by unsteady aerodynamic phenomena around the wings such as leading-edge vortices that arise and vanish over the flapping cycle [3]. It would result in high lift, and the viscous force will grow in comparison to inertial effects. Fixed-wing aircraft generate force in a horizontal direction, producing lift while generating a large amount of drag. As a result, flapping-wing robots produce lift more directly than fixed-wing aircraft. When compared to rotorcrafts, which are very energy-inefficient [4], flapping-wing robots could stay airborne for longer. Additionally, flapping-wing robots could also be quieter, thus more suitable for spying for military use. Rotorcrafts are usually very dangerous due to the high rotational speed of the propellers. When the rotorcraft is out of control, it would easily hurt people, not to mention that its propellers have the potential to kill people when fully functioning. Flapping-wing robots are safer since even the robot hits a person, the flapping motion of the wings will not cause any damage to that person. Therefore, flapping-wing robots are more human-friendly, easier to be accepted by the public. In terms of space technology, flapping-wing robots can be used outside of Earth, on other planets such as Mars [5]. They are more suitable for Martian flights because of the extremely thin Martian atmosphere which provides a harsh environment for traditional rotorcrafts. Since flapping-wing robots utilize air more efficiently, their flights can be achieved more easily on Mars.

Such benefits had interested many researchers since a copy of the hummingbird would be helpful to humans in many ways. Many of the researchers have successfully built different versions of flapping-wing robots. Some were able to hover and perform free flights for a few minutes. Three students from Purdue University investigated extreme hummingbird maneuvers on flapping-wing robots (Fig. 1a) [6]. They developed a 12g robot with only two actuators. The robot could carry out most of the maneuvers performed by its natural counterpart. The Nano Hummingbird, a light weighted, two-winged flapping-wing robot, was developed by AeroVironment in 2011 (Fig. 1b) [7]. The robot has a wingspan of 16cm and weighs only 19g. It is equipped with motors, batteries, control systems, and a video camera. It is able to fly forward at a maximum speed of 10m/s. It could hover stably and perform different agile maneuvers such as a 360-degree loop. The control distance is about 1km. Some researchers developed the robot differently. All the examples given above are two-winged. There is a four-winged flapping-wing robot developed by DelFly (Fig. 1c) [8]. The robot could hover for more than 5 minutes on a fully charged battery, with only a 17Hz wingbeat frequency. It weighs 29g and has a wingspan of 33cm. It could also perform flexible movements like a fly. Its maximum speed is 7m/s. Besides these three extraordinary examples, many other researchers also spent years in this area and eventually achieved some outstanding developments.

(a) (b) (c)

Fig. 1. Prototypes of present flapping-wing robots: (a) Hummingbird Robot by Purdue [6], (b) Nano Hummingbird by AeroVironment [7], and (c) DelFly Nimble [8].

To clarify, a flapping-wing robot described above is different from an ornithopter. FW-MAVs do not simply flap their wings up and down like birds. They mimic the flight of hover-capable insects or hummingbirds. The trajectories of the FW-MAV's wing's trailing edge and the wing tip are different and more complicated than those of the ornithopter. Another significant difference is that FW-MAVs control pitch, yaw, and roll motions by changing their wings' flapping motions whereas ornithopters are usually tailed with control surfaces.

In this report, I examined how to produce the most lift for my flapping-wing robot by conducting experiments with different independent variables (voltage, motor type, wing area, and the number of veins). The final version of the robot could produce more than 160N of lift since the robot (weighs 16.3g) is able to overcome its gravity and exert an upward trend. In all experiments, I used a pressure sensor to monitor the lift produced by the robot. I changed the voltage, the motor type, the wing area, and the number of veins in each wing to find out which design could produce the most lift. My goal is that the robot could hover with an onboard power source for at least one minute. I designed the control mechanism but was not able to integrate it with the robot because of its extra weight. In the future, I will optimize the structure of the robot to produce more lift and add the control system and an onboard power source to the robot.

The report is organized as follows. Section II describes the theoretical model that I develop my robot based on. Section III describes the development of my prototypes, the design of the structures and the wings, and the features of my final version of the robot. Section IV details the four groups of lift experiments that I conducted to optimize my design and the results and discussions of the experiments. Section V states my future expectations of the robot. Section VI concludes the paper.

II. THEORETICAL MODEL

The unsteady blade-element theory (UBET) was used to estimate the force generation in each direction for the wings of the flapping-wing robot and the power required for the robot to flap its wings [9-11]. Five force components are acting on the wings: translational force (dF_T), added-mass force (dF_A), rotational force (dF_R), inertial force (dF_I), and force due to the clap-and-fling effect ($dF_{c\&f}$) (Fig. 2). However, the UBET model cannot account for the force due to the clap-and-fling effect, so only the other four force components are calculated. The force generated by the wing in a given amount of time t in the η direction, which is tangential to the stroke plane and the force generated in the ζ direction (lift), which is vertical to the stroke plane are calculated below:

$$dF_\eta(t) = dF_{T\eta}(t) + dF_{A\eta}(t) + dF_{R\eta}(t) + dF_{I\eta}(t) \quad (1)$$

$$F_\zeta(t) = dF_{T\zeta}(t) + dF_{A\zeta}(t) + dF_{R\zeta}(t) + dF_{I\zeta}(t) \quad (2)$$

The power that the wings required to overcome the force in the horizontal direction in a given amount of time t can be calculated using the following equation:

$$dP(t) = \psi \times (\vec{r} \times \overrightarrow{dF_\eta}(t)) \quad (3)$$

Since the flapping-wing robot might not spend any of its power to rotate its wings around the ξ axis, the power can be neglected here [9].

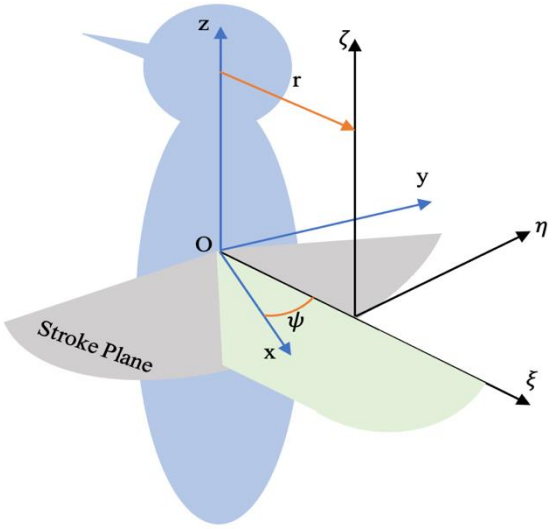

Fig. 2. Definition of the coordinate system [10].

III. MECHANICAL STRUCTURE

a) Overall Structure

The robot's structure is divided into four parts: the driving system, the motion transmission unit, the wings, and the control system. In my prototype, a coreless motor is chosen for the driving system. The motion transmission unit transmits the torque produced by the motor to the wings, converting the rotary motion into the reciprocating motion to drive the wings, thus lifting the robot. The motion transmission unit is comprised of gear transmission and a slider-crank mechanism. The wings produce lift for the robot. The control system is used to control the motion of the robot during flights. The control board could sense the displacement of the robot and send signals to the servos to maintain the robot's stability using a close feedback loop. Besides, by controlling the angle of the wings, the robot could theoretically achieve pitch and roll motion.

b) Driving System

A flapping-wing robot produces lift by flapping its wings. In order to drive its wings, a driving part becomes necessary. Since the robot has to overcome its gravity to fly, I need to keep its mass as low as possible. Therefore, a coreless motor (Fig. 3), which has a small mass and a high rotational speed, was chosen as my driving part. Other common driving parts for FW-MAVs are piezoelectric actuators and electromagnetic actuators [12]. Both are usually used for smaller flapping-wing robots in pico-scale, so they are not suitable for my model.

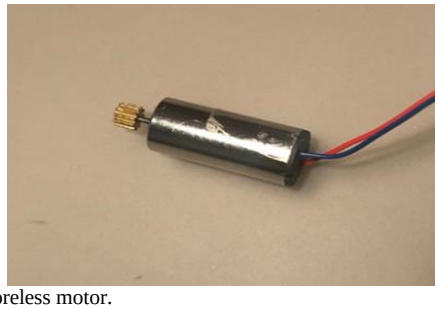

Fig. 1. A coreless motor.

c) Design of the Motion Transmission Unit

i.Synchronous Belt

Initially, I decided to use synchronous belts to transmit torque (Fig. 4a). A pulley with a diameter of 20mm and two spur gears with diameters of 10mm and 13mm were used in this design (Fig. 4b). The distance between the center of the outer gear and the center of the pulley is 15mm. The shaft of the motor is attached to the 10mm-diameter gear. The 13mm-diameter gear is attached to the smaller one to reduce the rotational speed. One end of the crank is attached to the bigger gear while the other end is connected to the pulley. Two synchronous belts are attached to the pulley. Each is wrapped around one of the wing mounts. I drew the structure using SolidWorks, then converted the files into AutoCAD and printed them out using a laser cutter. The components were then assembled. 2.5mm wood was used as the material. Since the two synchronous belts have to cross each other, the friction created by the contact was too big. When the motor started working, the belts could not move smoothly, thus failing to transmit torque. So, I decided to use a different way to achieve this goal.

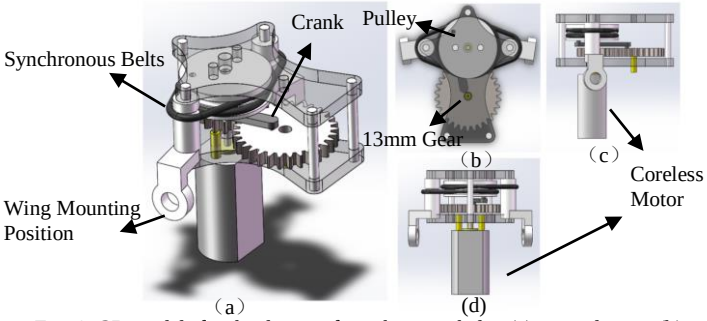

Fig. 4. 3D models for the design of synchronous belts: (a) general view, (b) top view, (c) side view, and (d) front view.

ii.Gear Drive

Using gears could also transmit torque. The design is presented in Fig. 5. A group of spur gears is used to slow down the rotational speed of the motor (Fig. 5b). The crank is connected to the biggest gear using a shaft, converting the rotary motion into the reciprocating motion. The other end of the crank is connected to another big gear, which has a smaller gear on top of it coaxially. The smaller gear is attached to another small one to mirror the motion of the big gear. The second small gear also has a bigger gear, the same size as the previous one, on the top coaxially. Each of the big gear is attached to one side of the gear that controls the motion of the wings. Thus, the two big gears are moving in the opposite directions, causing the two wings to flap in a mirror image. I printed out this version but found out that the two wings have very different stroke amplitudes. Gaps exist between each gear, so when transmitting torque, the wing attached to the first big gear will have a bigger stroke amplitude than the other wing. When reversing the direction of the motion, every tooth in the gears has to move a little bit – the gears are in clearance fit – because of the reciprocating motion. Since there are a lot of gears, all the gaps accumulate so that the stroke amplitudes of the two wings are very different. The wingbeat frequencies of the two wings are different too. The structure is too complicated for maintenance and could not amplify the stroke amplitude as much as other designs. Helical gears would be suitable for this design, but it was very hard to get any helical gears in such small sizes. Therefore, I decided to build new models.

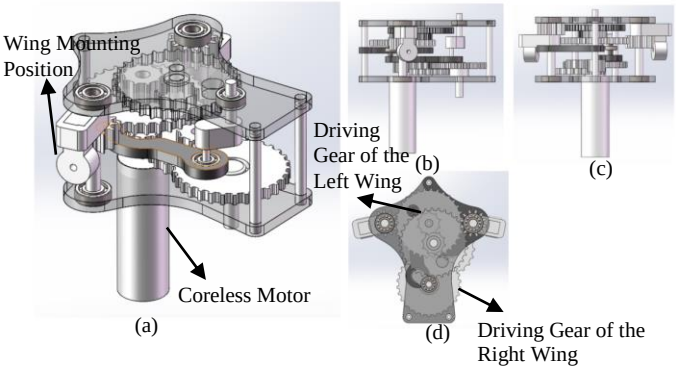

Fig. 2. 3D models for the design of gears: (a) general view, (b) side view, (c) front view, and (d) top view.

iii.Slider-Crank Mechanism

Another way to transmit torque is by directly connecting the crank to the shaft of the motor. Then the crank and the two swing arms are stabilized by one shaft that goes through all three components. The swing arms are 20mm in length. The structure will also convert the rotary motion of the motor to the reciprocating motion of the wings. However, this structure has a few problems. The shaft that goes through the crank and the swing arms would sometimes fall out if the motor spins too fast. Besides, they could never stay on the slide that was designed since the shaft would not move in a line. Therefore, another connecting link might be needed to connect the crank and the shaft. One end of the connector is going to move in a line, in accordance with the slide. Connecting that end of the connecting link to the swing arms would solve the problem.

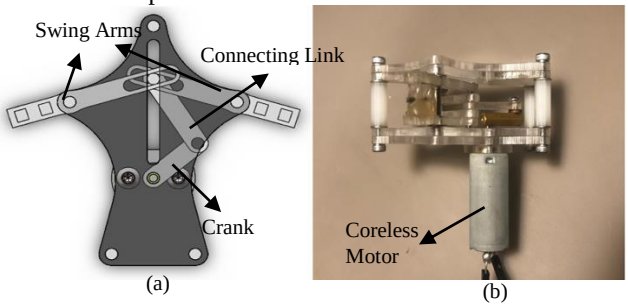

Fig. 3. Slider-crank mechanism: (a) top view of the 3D model and (b) side view of the prototype.

Thus, a slider-crank mechanism is needed to transmit torque (Fig. 6). Since the stroke amplitude should be as big as possible to produce as much lift, the length of each component in the slider-crank mechanism is calculated. When the crank and the connecting link reach collineation, the swing arms will reach their limiting position. There are two situations in which the crank and the connecting link are on a line. The angle between the two limiting positions of the swing arms is the stroke amplitude of the robot.

$$\cos\theta_1 = \frac{R_2^2 + 15^2 - (L - R_3)^2}{2 \times 15 \times R_2} \quad (4)$$

$$\cos\theta_2 = \frac{R_2^2 + 15^2 - (L + R_3)^2}{2 \times 15 \times R_2} \quad (5)$$

$$\theta = \theta_2 - \theta_1 \quad (6)$$

R2 is the length of the swing arms. R3 is the length of the crank. L is the length of the connecting link. θ is the stroke amplitude.

In my first version of the slider-crank mechanism, the crank is 30mm long. The distance between the crank and the swing arms is 110mm. The swing arms are 60mm long. The connecting link is 140mm long. The stroke amplitude is about 60 degrees, but the distance traveled by the crank and the swing arms is too long, and the stroke amplitude might be too small. I decided to adjust the length of the crank and the swing arms. The second version of the slider-crank mechanism has a 20mm crank. The length of the swing arms is 50mm. The connecting link is 130mm long, and the distance between the crank and the swing arm is kept unchanged, 110mm. The stroke amplitude is calculated as following using equations (4), (5), and (6):

$$\cos\theta_1 = \frac{50^2 + 110^2 - (130 - 20)^2}{2 \times 110 \times 50} = \frac{5}{22} \quad (7)$$

$$\theta_1 = \cos^{-1}\frac{5}{22} = 76.77° \quad (8)$$

$$\cos\theta_2 = \frac{50^2 + 110^2 - (130 + 20)^2}{2 \times 110 \times 50} = -\frac{79}{110} \quad (9)$$

$$\theta_2 = \cos^{-1} -\frac{79}{110} = 135.79° \quad (10)$$

$$\theta = \theta_2 - \theta_1 = 135.79° - 76.77° = 59.02°$$

I thought this version of the slider-crank mechanism would work well because the distance traveled by the crank and the swing arm is within the range. This version was printed using a laser cutter and was assembled.

I optimized the structure based on the problems that I encountered in the previous version. The length of each component in the slider-crank mechanism is reset. The crank is now 35mm long, the swing arms 50mm, the connecting link 160mm, and the distance between the crank and the swing arm is 150mm. This design increased the stroke amplitude to 98.95degrees, and it could work well with a motor spinning at high speed during testing. The wings were attached to the structure. The first flight test was performed, but I found out that the torque produced by the motor was too big. The wings had very high frequencies but could not withstand such dramatic flapping, so they broke apart. No material could withstand the torque produced by the motor even with the support of the carbon fiber rods. Therefore, I decided to slow the motor down when transmitting torque by using gears.

I used four spur gears to transmit torque and reduce the rotational speed (Fig. 7). The number of teeth(z) of the smallest gear is 8. The gear that is attached to the first one has two layers; one smaller gear with a z of 10 on the top and a smaller gear with a z at the bottom. Both gears are coaxial and are not separable. The top of the second gear is attached to a third gear, which has a bigger gear with a z of 26 on the top and smaller gear with a z of 10. The bottom of the third gear is attached to the last gear, which has a z of 30. The diameters of the gears are 5mm, 12mm and 6mm, 14mm and 6mm, and 16mm. The gears have a transmission ratio of 20/429. The wingbeat frequency of the robot is 39Hz under 3.7V (see appendix A). The wingbeat frequency of a hummingbird is between 22-78 Hz [13]. When increasing the voltage to 9V, the wingbeat frequency of my robot is going to increase. When the motor is spinning alone, the wingbeat frequency could reach 39Hz, but the actual wingbeat frequency at 3.7V is going to be lower since different components in the robot will produce resistance to the motor. After considering all these factors, the robot's wingbeat frequency would be within the range of the wingbeat frequency of a real hummingbird.

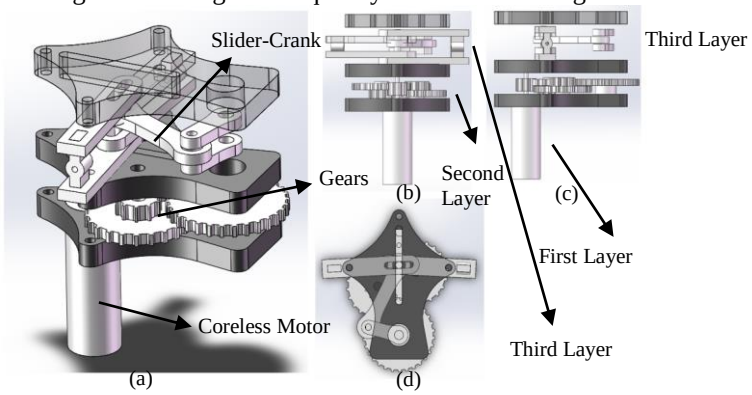

Fig. 4. 3D models for the combination of slider-crank and gears: (a) general view, (b) front view, (c) side view, and (d) top view.

The wings were able to function well on this version. However, the structure was not stable enough. In this situation, only one shaft is able to go from the top layer to the bottom layer. On the other side – the board that separates the layers are symmetric in shape– the shaft could only go halfway through since it will interfere with one of the gears if it penetrates the whole structure. Based on previous testing, the structure would sometimes fall apart. Sometimes the top layer and the bottom layer would separate because of the dramatic flapping motion of the wings. On the other side, the length of the shaft is equivalent to the gap between the top board and the board below it. When the wing flaps, the shaft that does not fully penetrate the two boards will easily fall off because of the vibration of the robot. To solve this problem, the size of the boards was modified. The shafts were placed farther from each other so that they would not interfere with the gears. Since the swing arms are fixed to the shafts, they are also extended. This would decrease the stroke amplitude slightly but strengthen the structural integrity of the robot. Other parts of the structure are kept unchanged.

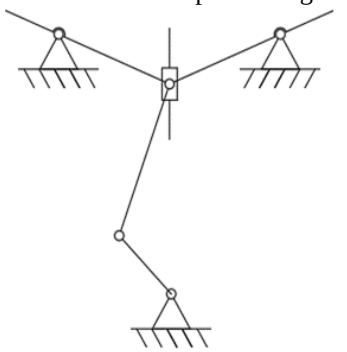

Fig. 5. Slider-crank mechanism.

iv.Material Analysis

All the previous designs were made of either wood or acrylic (Fig. 9). Both are quite light, but not strong enough.

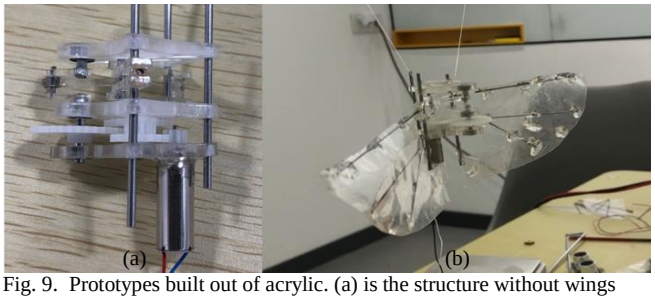

Fig. 9. Prototypes built out of acrylic. (a) is the structure without wings whereas (b) is the prototype during tests.

When increasing the voltage to 6V, some components would cease functioning or fall apart. The crank has broken several times under high voltage conditions. Through force analysis, I was able to find out the forces that caused the failure of the crank (Fig. 10). F_1 is the force acting on the crank. F_2 is the force acting on the left swing arm by the connector. F_3 is the force pulling the shaft that goes through both swing arms and the connector. θ_1 is the angle between F_1 and F_2 whereas θ_2 is the angle between F_2 and F_3. Using F_3 as the reference force, F_1 and F_2 can be calculated as follows:

$$F_1 = \frac{F_3}{\cos\theta_1} \quad (11)$$

$$F_2 = \frac{1}{2} \times \frac{F_3}{\cos\theta_2} \quad (12)$$

θ_1 will always be bigger than θ_2, thus F_1 would always be greater than F_2. I was only able to see the failure of the crank because it was experiencing the most force. The failure of the swing arms might appear if the voltage was higher because the force from the shaft was acting on the thin side of the swing arm, which was only about 1mm wide. 6V wasn't enough for the robot to produce enough lift. Under higher voltage, the structural integrity of the crank and the swing arms needed to be enhanced. During flight tests, the top board sometimes would be detached from the body. Since the two swing arms were placed on top of each other, during reciprocating motion, they sometimes would crash into each other. The top swing arm would then hit the top board, causing an upward force that might separate the body and the top board. Besides, as the wings were always producing lift, the lift would directly act on the swing arms to which the wings were attached, further increasing the upward force that cause the top board to detach from the body. Due to all these problems, I decided to replace acrylic with carbon fiber, which is a lot stronger. In addition, carbon fiber is also very light, about the same mass as the acrylic material that I used. Structures made of carbon fiber could work well even during high voltage tests. I used the carbon fiber components that I got from an outside factory to assemble a new version.

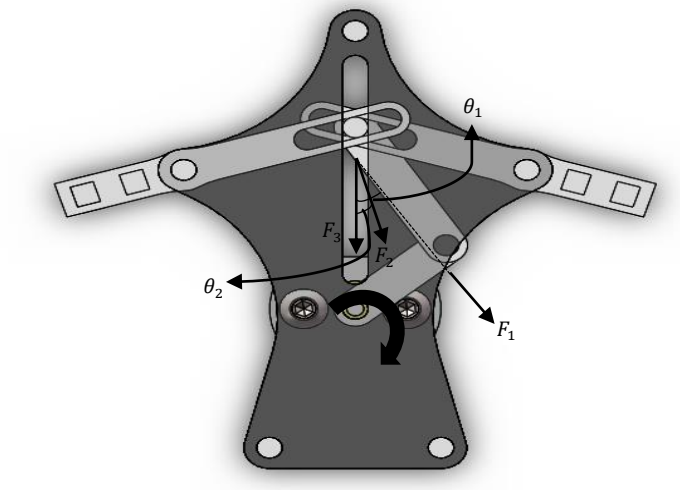

Fig. 10. Force components acting on the body of the robot.

v.Final Version

The final version of my robot weighs 16.3g. The main structure is made of carbon fiber. All the carbon fiber boards are 3mm thick while the components such as the crank and the swing arms are 1.5mm thick. The main structure had four layers, separated by three boards. The coreless motor labeled 8520 with a diameter of 8.5mm and a height of 20mm has a rated power of 3W and a rated speed of 50000rpm. Its rated voltage is 3.7V. The motor is attached to the bottom carbon fiber board. There is a hole on the board so that the motor could fit in there (interference fit). A small gear is attached to the shaft of the motor. Four spur gears are used to transmit the torque produced by the motor and reduce the rotational speed. The design of the gears was kept unchanged since the third version. The shaft that goes through the biggest gear is also in the third layer, where the slider-crank mechanism is placed. The shaft goes through a bearing on the second board to reduce friction. One end of the crank is attached to the shaft while the other end is attached to another shaft. The shaft is attached to a 20mm connecting link that connects the crank and the swing arms. There are two 24mm swing arms; each is connected to one wing. The swing arms are composed of the upper part and the lower part. They were connected by a small rectangular component with a tiny hole on it. The main carbon fiber rod of the wing goes through the tiny hole so that the wing is connected to the body of the robot. On the second board and the third board, there are two 17mm slides. One shaft goes through the two swing arms and the connecting link and moves along with the slide. The rotary motion of the motor is converted to the reciprocating motion through the slider-crank mechanism in the third layer of the main structure. The third board closes the third layer on the top. There are two shafts on each side that goes through all three layers to stabilize the whole structure. Fig. 11 shows the CAD drawing of the design while Fig. 12 is the final version of the robot. Each wing is made of 0.025mm PET material and is supported by three carbon fiber rods. Two of them have 0.5mm diameter while the main one at the leading edge has a 1mm diameter. The wings are in a shape similar to a 90-degree sector from an oval. The final version of the robot is small and light weighted. (Fig. 12). Its sketch was created using SolidWorks first then was converted into AutoCAD. CAD files were sent to an outside factory for laser cutting. The carbon fiber components were then assembled into the flapping-wing robot.

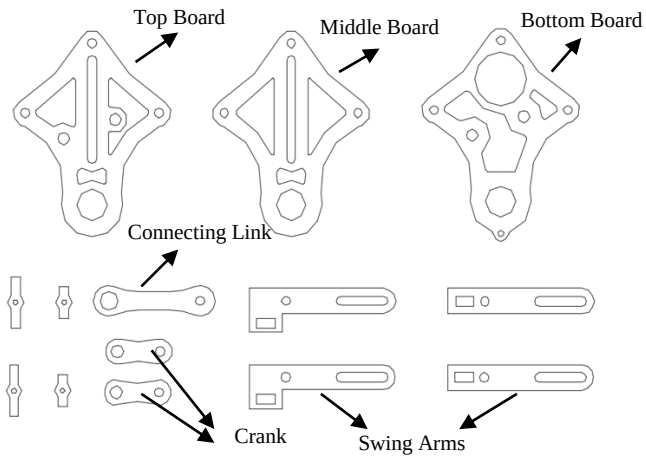

Fig. 6. CAD drawing of the final design. Sketch was created using AutoCAD.

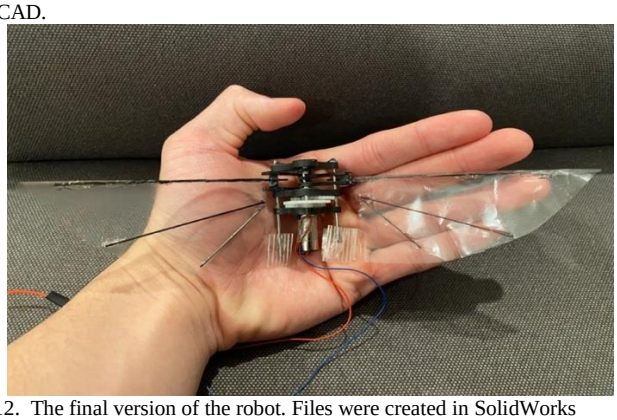

Fig. 12. The final version of the robot. Files were created in SolidWorks first then Converted into AutoCAD for laser cutting.

d) Design of the Wings

Since the robot's wings are placed vertically to the ground, in order to produce lift, the bottoms of the wings have to be fixed. They are connected to the main body since only the upper part of the wings should be moving back and forth. Thus, the wings are always producing lift whether during upstroke or downstroke, and they are always flapping at an approximately 45-degree angle. The wing will exert a downward force. According to Newton's third law, for every action, there is an equal and opposite reaction. When the wing exerts a force on the air, the air exerts an upward reaction on the wing, thus producing lift. The larger the stroke amplitude, the more lift the robot will produce. With greater deformation of the wing, the robot will also produce more lift. The wings of an insect have three different layers: each with a different thickness. The layer closest to the body is the thickest and the one farthest from the body is the thinnest, allowing the edge of the wing to deform freely to produce more lift or achieve more complex maneuvers. It was very hard for us to mimic the characteristics of a real insect's wing because I could not create varied thicknesses while keeping the wing surface smooth. New designs were created to simplify a real insect's wing.

Two designs of the wings were drawn. The first design of the wing is in an isosceles trapezoidal shape with three 0.5mm carbon fiber rods on each side of the shape. At the leading edge of the wing, there is a 1mm carbon fiber rod that is connected to the body. There are two other 0.5mm carbon fiber rods glued to the diagonal of the isosceles trapezoid. With these six carbon fiber rods, the wing is very strong. It can endure quite a large amount of force exerted on the wing during flapping motion. Since the carbon fiber rods are very thin, they are easy to deform but still very hard to break. Therefore, the deformation of the wing in this design is carried out by the carbon fiber rods because the wing folds vertically, and the carbon fiber rods are placed at a 40-degree angle. The veins will not experience all the vertical force, but at least part of it. The wing root is cut at about a 30-degree angle. The area being cut will produce drag instead of lift [14]. With that area, the robot will consume more energy to flap its wings. So, that area is cut for this version of the wings.

The other design is similar to the shape of a bird's wings, a sector from an oval shape. There is a 1mm carbon fiber rod at the leading edge of the wing that connects it to the body. One end of the other two 0.5mm carbon fiber rods are placed in the same place, but they have different angles: 3 degrees and 48 degrees. Each carbon fiber rod does not reach the trailing edge of the wing since I want part of the wing to move freely. There is a 1cm gap between the end of the carbon fiber rods and the trailing edge of the wing. Since the veins are placed horizontally, they will not endure the vertical forces produced by the deformation of the wings during flapping motion. The wing material is easier to deform than the carbon fiber rods. So, this wing design is theoretically more reasonable than the first one. My initial design has a wing area of $2493mm^2$. Later, two more pairs of wings were made according to this design. They have the same structure but have bigger areas: $3592.8mm^2$and $5933.4mm^2$ (Fig. 13).

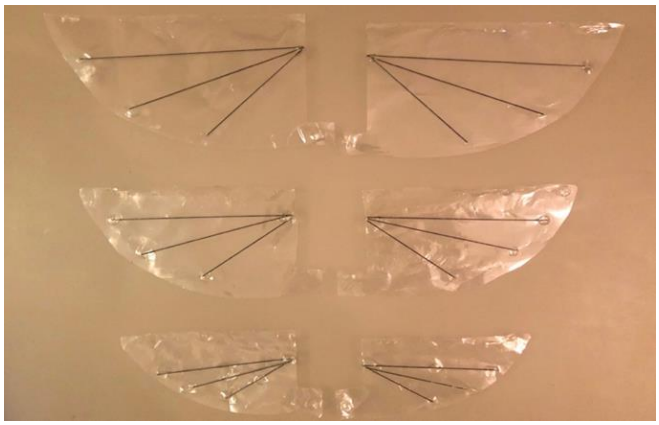

Fig. 7. Wings with wings areas of $5933.4mm^2$, $3592.8mm^2$, and $2493mm^2$. Wings with $2493mm^2$ wing area was chosen in the final version.

Based on the second design, I investigated the best material for the wing. 0.025mm polyethylene terephthalate (PET), 0.2mm polyvinyl chloride (PVC), and 0.2mm tear-resistant nylon was selected for the wings. Among these three materials, PET is the softest, and nylon is the hardest, thus PET will have the greatest deformation during flapping motion, and nylon will be hard to deform but also hard to break.

The shape of the wing was printed out using a laser cutter on a plank. 0.025mm PET was chosen as the wing material. The plank was glued to a sheet of PET material. The shape of the wing was then cut out, and the carbon fiber rods were glued to the wing using UV glues. Two pairs of wings were made according to each design.

For my final version, I initially used PVC material because it was very strong though had a limited ability to deform. Since the robot is going to work under high voltage, PET material might be torn apart during flight tests. However,

the lift produced by the PVC wings was only 4 to 5g under 9V. It is about the same lift produced by the previous version made of acrylic with the PET wings under 5V. Therefore, I decided to replace the PVC wings with the PET wings in order to gain more lift. The lift is 10g under 9V with PET wings, and the wings were intact. Therefore, PET is the most desirable material among the three for the wings of a flapping-wing robot.

e) Control Mechanism

Two servos were used to control the roll and pitch motion of the robot (Fig. 16). Since the roll motion and yaw motion are similar to certain degrees, I did not consider the yaw motion here because it would add more weight to the robot. The pitch motion of the robot is controlled by the top servo whose arm is attached to the end of the base of the robot by tilting the stroke plane in the z-direction (Fig. 16a). When the stroke plane is tilted downward, the wings are able to generate a forward thrust that allows the robot to fly forward (Fig. 17a). The roll motion is controlled by the bottom servo whose arm is attached to the side of the base of the robot (Fig. 16b). Similarly, when the stroke plane is tilted to the right, the wings are able to generate a force to the right so that the robot could roll to the right (Fig. 17b).

Two 3.7V batteries are installed at the bottom of the structure in a series connection. They could produce a maximum of 7.4V during flapping motion. There are two battery mounts to fix the batteries so that they would be static during flights. Two separate wires are attached to the battery. One is used for charging; the other one is used to connect to the receiver. A switch is also installed at one end of the base to control the batteries (Fig. 14).

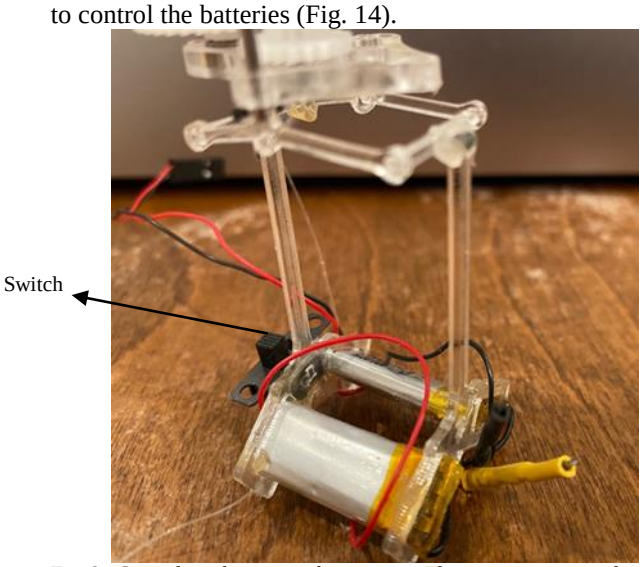

Fig. 8. Control mechanism without servos. The structure was made of acrylic. The control system was manufactured and tested but was not able to be added to the final version of the robot due to the insufficient lift produced.

Fig. 9. The Remote control that can be used to control the motion of the robot if the control system is properly installed.

When doing lift experiments, I used a version without the control systems because my robot was not able to produce sufficient lift even without the control systems during flight tests. The control system weighs 17g, which will cause the total weight of the robot to exceed 30g. Besides, the control board that I have has not been completely set up yet, so the robot could not achieve self-stabilization even with all the electrical devices installed. If the control board is properly installed and well-coded for controlling the servos and the motor, with sufficient lift, theoretically, the robot could achieve free flight with the remote control that I have already prepared (Fig. 15).

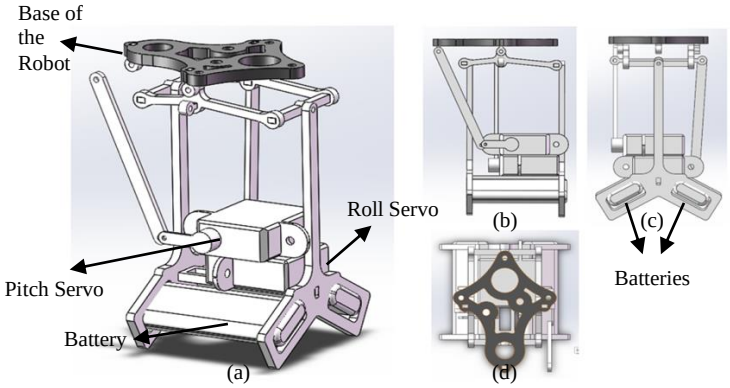

Fig. 10. 3D model of the control mechanism with servos and batteries: (a) general view, (b) side view. (c) front view, and (d) top view.

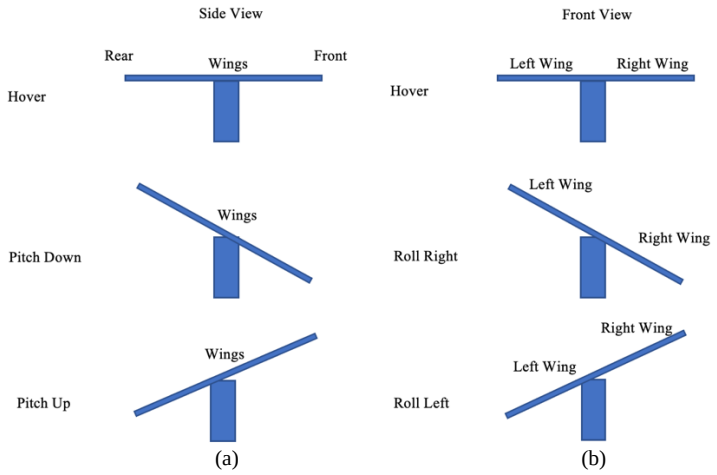

Fig. 17. Working principles of the control mechanism: pitch (a) and roll (b) [15].

IV. LIFT EXPERIMENTS

Four groups of experiments with different independent variables were conducted to test factors that would affect the

lift produced by the flapping-wing robot. During this phase of research, my robot was still made of acrylic instead of carbon fiber. The wings were made of PET material since based on previous testing, PET appears to be the best material to maximize lift. The mass of the robot during experiments was 13.4g. Among all the factors that are going to be investigated, increasing some – for example the voltage and the wing area – seems to increase the lift produced by the robot. However, increasing these values would cause more problems, such as the uncontrolled vibration of the robot and the increasing resistance exerted on the wings. These experiments were performed to find a balance in these values to maximize the lift while ensuring the robot is in a safe situation. The lift was monitored by a 5kg pressure sensor (HX711 module) at the top of the frame, which was used to hang the robot. The sensor was connected to a PC with Arduino installed, so the value that the sensor detected was displayed on the computer (Fig. 18a). First, the robot was put on a scale to measure its weight which is 13.4g. Then, one end of the rope was tied to the bolt on the sensor, and the rope was used to hang the robot. I always waited until the value displayed on the PC was stable at 0g. After I got the data from the pressure sensor, I converted them into lifts by doing simple calculations. I examined the relationship between the voltage and lift, the wing area and lift, the motor type and lift, and the number of veins and lift. For each group of the experiment, the setups are all the same as described above. Three trials were performed for each group of variables.

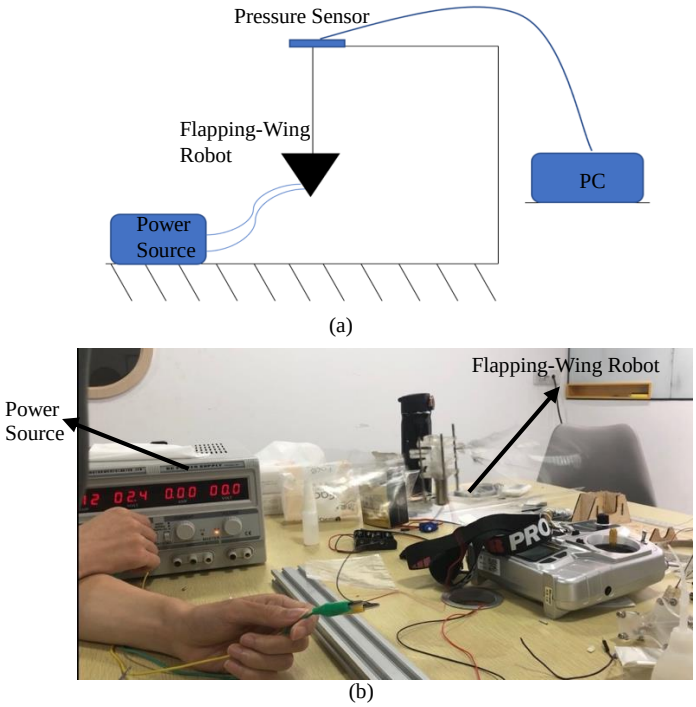

Fig. 11. Experimental setup. Four groups of lift experiments were performed; each with three treatment groups and three trials. (a) is the sketch of the setup. (b) is a photo taken during a test.

A. *Voltage vs. Lift*

When examining the relationship between the voltage and the lift that the robot produced, the wing area ($2493mm^2$), the number of veins, the motor, the transmission ratio which was 1:21.45, the structure of the robot, the shape of the wing, the material of the wing, the power source, the sensor, and the flapping time which is 10s were kept the same. The voltage was increased to 2V, and the wings flapped for 10 seconds. The highest lift that was produced by the robot over the 10-second interval was recorded. The process was repeated three times. All the values were averaged, and the average absolute deviations (AADs) were calculated. I did 2V, 3V, and 4V to compare the effect of the voltage on the lift. As the voltage increased from 2V to 3V, lift increased by 16.7N (Fig. 19). When the voltage increased from 3V to 4V, lift decreased by about 5N. As the voltage increase, the wingbeat frequency would increase accordingly, thus producing more lift. With high wingbeat frequency, the robot would vibrate more dramatically. When it could not balance itself, part of the lift produced by the wing would be canceled by the irregular vibration. Therefore, the lift would decrease instead. To maximize the wingbeat frequency and simultaneously keep the robot's balance, 3V is the best voltage for testing. In later testing, the voltage was increased to 9V so that the robot made of carbon fiber was able to overcome its gravity. Under 9V, the robot would experience strong vibration theoretically, but it is still able to stabilize itself. It is similar to a Kapitza's pendulum, which is an inverted pendulum with a vertically vibrating pivot point [16]. The pendulum can be stabilized through high frequency and small amplitude vibration. The flapping-wing robot also utilizes this effect to stabilize itself under 9V. This effect might be inconspicuous when the voltage is too low, for example, 3V or 4V.

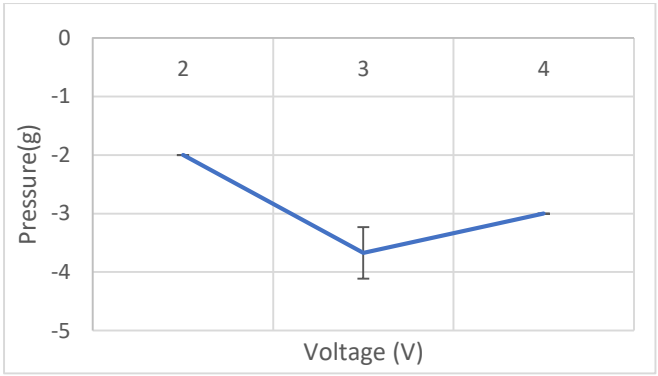

Fig. 12. The relationship between voltage and pressure. Three treatment groups (2V, 3V, and 4V) were conducted by changing the voltage of the power source, and there were three trials within each treatment group. The lift was monitored by the pressure sensor. Error bars represent AAD.

a) *Motor vs. Lift*

When examining the relationship between the diameter of the motor and the lift that the robot produced, the voltage which was 3V, the number of veins, the wing area ($2493mm^2$), the transmission ratio which was 1:21.45, the structure of the robot, the shape of the wing, the material of the wing, the power source, the sensor, and the flapping time which is 10s were kept the same. First, a motor named 716 was used, meaning that its diameter was 7mm. The wings flapped for 10 seconds. The highest lift that was produced by the robot over the 10-second interval was recorded. The process was repeated three times. All the values were averaged and the AADs were calculated. Three different kinds of motors (716(7mm), 816(8mm), and 8520(8.5mm)) were used to compare the effect of the motor on the lift. As the diameter of the motor increased, the lift produced by the robot also increased. 716 produced an average of 36.7N of lift while 8520 produced an average of 46.7 N of lift (Fig. 20). As the radius of the motor increased, the nominal power of the motor increased, thus the wingbeat frequency of the robot was increased. Under only 3V, the robot was in a good situation where it could maintain its balance to some extent.

Thus, even though the frequency of the robot increased, it could still increase the lift without losing its balance. Using a stronger motor would help to increase the lift. 8520 might be the most suitable motor that I could find so far. A bigger motor would increase the weight of the robot, so bigger motors that produced a larger amount of lift will not help either. Besides, the structure probably could not endure more dramatic flapping. As a result, 8520 would be used as the motor for my final version of the robot.

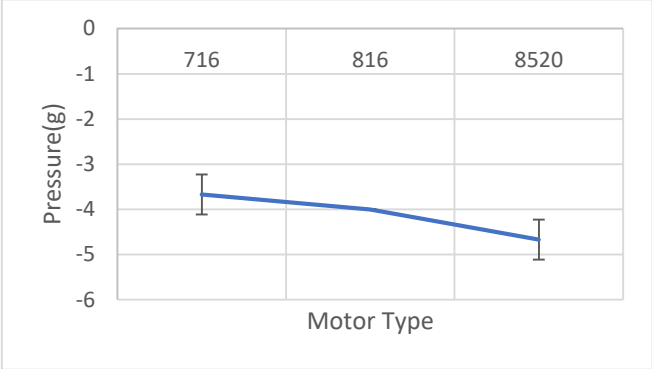

Fig. 13. The relationship between motor type and pressure. Three treatment groups (716 motor, 816 motor, 8520 motor) were conducted by replacing different motors in the robot, and there were three trials within each treatment group. The lift was monitored by the pressure sensor. Error bars represent AAD.

b) Wing Area vs. Lift

When examining the relationship between the wing area and the lift that the robot produced, the voltage which was 3V, the number of veins, the motor, the transmission ratio which was 1:21.45, the structure of the robot, the shape of the wing, the material of the wing, the power source, the sensor, and the flapping time which is 10s were kept the same. First, wings with an area of 2493 mm^2 were used. The wings flapped for 10 seconds. The highest lift that was produced by the robot over the 10-second interval was recorded. The process was repeated three times. All the values were averaged and the AADs were calculated. Wings with three different areas (2493mm^2, 3530mm^2, and 5933mm^2) were used to compare the effect of the wing area on the lift. The 2493mm^2 wings produced the highest lift, which was 46.7N while the 3530 mm^2 wings and the 5933 mm^2 wings produced less lift, 33.3N (Fig. 21). As the wing area increased, the lift produced by the robot decreased. A bigger wing area means bigger wing inertia. Bigger wings would consume more energy in order to reach the same wingbeat frequency as smaller wings. When the voltage was kept at 3V, and the motor was the same, bigger wings would have a lower wingbeat frequency. The effect of the wingbeat frequency on the lift is more significant than the wing area. Thus, smaller wings with higher frequency would produce more lift than bigger wings with lower frequency. The 2493 mm^2 wings would be used for my final robot.

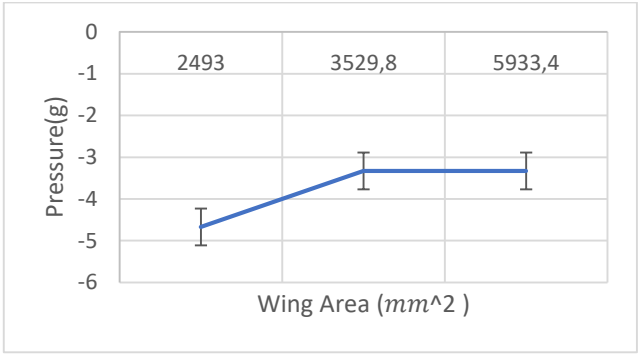

Fig. 14. The relationship between wing area and pressure. Three treatment groups (wings with 2493mm^2, 3530mm^2, and 5933mm^2) were conducted by replacing attaching different wings to the robot, and there were three trials within each treatment group. The lift was monitored by the pressure sensor. Error bars represent AAD.

c) Number of Veins vs. Lift

When examining the relationship between the number of veins and the lift that the robot produced, the voltage which was 3V, the motor, the wing area (2493 mm^2) , the transmission ratio which was 1:21.45, the structure of the robot, the shape of the wing, the material of the wing, the power source, the sensor, and the flapping time which is 10s were kept the same. First, wings reinforced by 4 carbon fiber rods were used. They flapped for 10 seconds. The highest lift produced by the robot over the 10-second interval was recorded. The process was repeated three times. All the values were averaged and the AADs were calculated. Wings reinforced by 4, 3, and 2 carbon fiber rods were used to compare the effect of the number of veins on the lift. When there were 3 carbon fiber rods, the wings produced an average of 36.7N of lift, the highest lift produced among the three groups (Fig. 22). Wings with 4 carbon fiber rods and 2 carbon fiber rods produced 26.7N and 23.3N of lift. There is no obvious trend of lift according to the variation of the number of veins. The carbon fiber rods limit the wing's ability to deform. With fewer carbon fiber rods, the wing could deform more freely, theoretically producing more lift. However, during flapping motion, wings with fewer veins would experience some irregular deformation. Such deformation might not produce lift but increase the drag instead. Therefore, even though wings with 2 carbon rods are easier to deform than wings with 3 carbon fiber rods, they still produce less lift. 3 carbon fiber rods might be the best structure for the wing, balancing the effect of wing deformation on drag and lift. 3 carbon fiber rods would be attached to the wings as vein reinforcement for the final version of the robot.

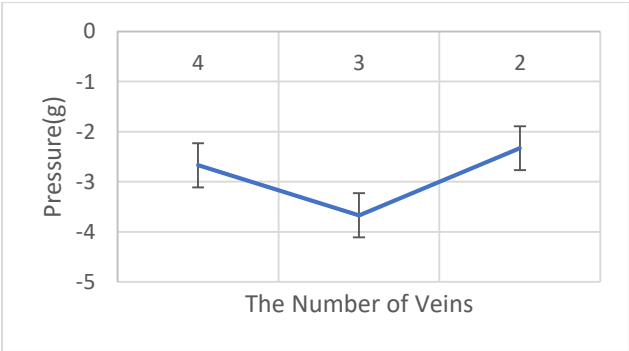

Fig. 15. The relationship between the number of veins and pressure. Three treatment groups (4 veins, 3 veins, and 2 veins) were conducted by adding different number of carbon fiber rods to the wings, and there were three trials within each treatment group. The lift was monitored by the pressure sensor. Error bars represent AAD.

d) Discussion

The lift produced by the robot is the most important factor that would affect its performance. Theoretically, the lift should exceed 134N – the robot's gravity – for it to fly. Through my experiments, I found out that a robot with the 8520 motor, 2493mm^2 wings, and 3 veins on the wings would produce the highest lift when working under 3V. The wingbeat frequency, the vibrating amplitude, and the deformation of the wings are in the best situation to produce lift. There is a difference between the data that I got because the experiments were performed on two separate days. On the first day, the data collected by the pressure sensor did not seem to be as accurate because even though I waited until the data was stable at 0g to start the experiments, there was still some fluctuation, ranging from 1g to -2g. The data collected on that day were generally higher. The actual lift that the robot produced might be about 1g lower. On the second day, the data were more accurate because some of the wires were reconnected. The data was able to keep unchanged at 0g when the robot was hanging still by the rope. To improve these, a more accurate pressure sensor should be used next time. The one that I used does not give decimal points. With two or three decimal points, the data would provide more information. Besides, reducing the vibration of the robot by using more ropes to hang the robot is also a possible way. The ropes would restrain the horizontal movements of the robot. In this way, the data that I collected is purely the robot's lift.

V. FUTURE WORK

Future work of the robot would be devoted to increasing the robot's lift by increasing the stroke amplitude of the wings, reducing the existing weight of the robot by optimizing its structure and adding an onboard power source and a flight control system.

The current version of the robot with no onboard power source only has a stroke amplitude of 98 degrees, providing enough lift for the robot under 9V. The robot needs an onboard power source for it to perform different tasks so that it could be utilized commercially. However, an onboard power source that could provide 9V will be too big and too heavy for an FW-MAV like this. Therefore, I need to lower the voltage barrier for the robot to produce enough lift. It would be possible to install a lower-voltage power source, which would decrease the wingbeat frequency of the robot. One way for the robot to maintain sufficient lift while reducing its wingbeat frequency is to increase the stroke amplitude so that it could utilize the clap-and-fling effect which will increase the lift produced by the wings (Fig. 23) [17]. Since the robot contains a slider-crank mechanism that converts the rotary motion of the motor to the reciprocating motion of the wings, I could increase the length of the crank to increase the stroke amplitude. With a longer crank, I would need a longer slide for the shaft to fit in. Since both the couplers to where the wings are attached are connected to the slider by a shaft, a longer slide will result in a bigger stroke amplitude. When the stroke amplitude is close to 180 degrees, the clap-and-fling effect would help produce extra lift so that the robot could overcome its gravity under a lower voltage. I also need to consider some other factors when increasing the stroke amplitude. The sizes of the three carbon fiber boards need to be modified to fit the new design. The increase in the size of the carbon fiber boards may also add weight to the robot, so I need to find a balance between the length of the crank and the size of the boards. With a bigger stroke amplitude, the wings would experience more resistance during flapping motion. However, since the wingbeat frequency is lower, the current design of the wings might still be able to perform well. Future experiments need to be performed to determine these factors.

The main structure of the current robot is made of carbon fiber, which provides high structural integrity but also increases extra weight compared to acrylic. Through experiments, I found out that only structures made of carbon fiber could withstand the strong vibration of the robot under 9V. Other materials such as acrylic would be damaged under 9V. If a robot with a larger stroke amplitude is able to produce enough lift under a lower voltage, I could replace the carbon fiber with acrylic, which was what I did in the first place. Replacing carbon fiber with acrylic could reduce a few grams of weight, and the robot will be easier for maintenance.

I already have a design for the control mechanism. The next step would be to implement the design to the robot with a larger stroke amplitude. The robot could produce more lift to sustain a hover flight with an onboard power source, servos, and auto-pilot. The weight reduced by replacing the material would be compensated by these electrical devices. The robot will have a similar weight as the current version.

Through these improvements, at best, the robot could perform hover-capable flight and free flight for a few minutes with an onboard power source.

VI. CONCLUSION

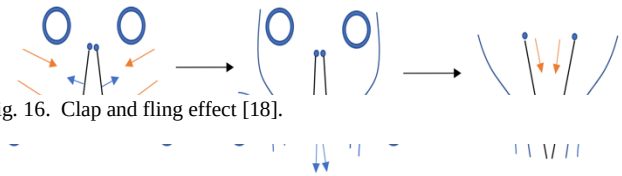

Fig. 16. Clap and fling effect [18].

I examined the mechanical design and factors that would affect the lift of a flapping-wing robot. My final version of the robot has a mass of 16.3g. It could generate more than 163N of lift under 9V. The wingbeat frequency of the robot reaches about 40Hz, almost the same as a real hummingbird. I improved the wings by optimizing the wing area, wing material, and veins. Meanwhile, I investigated the best motor and the best frame material for the robot. Now the robot is able to produce enough lift to overcome its gravity. However, I used an off-board power source for my robot instead of onboard batteries. The next step would be adding the batteries. The mass of the robot would increase about 3-4 grams, so I have to improve my model to produce more lift. Control mechanisms also need to be added to the robot. A fully functional flapping-wing robot like this could replace some of the current rotorcrafts which are very energy-inefficient. However, if a smaller and lighter onboard power source with a large capacity is not achievable, the commercialization of flapping-wing robots might not be possible in recent years.

APPENDIX A

The diameter of the gears is as below.

$$d_1 = (8 + 2) \times 0.5 = 5\text{mm}$$
$$d_2 = (22 + 2) \times 0.5 = 12\text{mm}$$
$$d_3 = (10 + 2) \times 0.5 = 6\text{mm}$$
$$d_4 = (26 + 2) \times 0.5 = 14\text{mm}$$

$$d_5 = (10 + 2) \times 0.5 = 6\text{mm}$$
$$d_6 = (30 + 2) \times 0.5 = 16\text{mm}$$

The transmission ratio i is calculated as below.

$$i = \frac{8}{22} \times \frac{10}{26} \times \frac{10}{30} = \frac{20}{429}$$

The rotational speed of the motor under its rated voltage (3.7V) is 50000rpm, so the rotational speed of the last gear is:

$$50000\text{rpm} \times \frac{20}{429} = 2331\text{rpm}$$

Since the wingbeat frequency is the same as the rotational speed of the last gear, the wingbeat frequency is:

$$\frac{2331\text{rpm}}{60\text{s}} = 39\text{Hz}$$

REFERENCES

[1] H. Li and S. Guo, "Aerodynamic Efficiency of a Bioinspired Flapping Wing Rotor at Low Reynolds Number," *Royal Society Open Science*, vol. 5, no. 3, 2018, pp. 171307, DOI: 10.1098/rsos.171307.

[2] E. Regis, "No One Can Explain Why Planes Stay in the Air," *Scientific American*.

[3] G. De croon, "Flapping Wing Drones Show off Their Skills," *Science Robotics*, vol. 5, no. 44, 2020, DOI: 10.1126/scirobotics.abd0233.

[4] R. Öhlund, "Drones and energy efficiency," *SmartPlanes*, 28 Nov. 2017, smartplanes.com/drones-and-energy-efficiency/. Accessed 29 Dec. 2021.

[5] J. A. Pohly, C. Kang, D. B. Landrum, J. E. Bluman and H. Aono, "Data-driven CFD Scaling of Bioinspired Mars Flight Vehicles for Hover," *Acta Astronautica*, vol. 180, pp. 545-559, 2021, DOI: 10.1016/j.actaastro.2020.12.037.

[6] F, Fei, Z. Tu, J. Zhang and X. Deng, "Learning Extreme Hummingbird Maneuvers on Flapping Wing Robots," *Arxiv*, 25 Feb. 2019, arxiv.org/abs/1902.09626.

[7] *Airforce Technology*. www.airforce-technology.com/projects/hummingbird-nano-air-vehicle/. Accessed 20 Dec. 2021.

[8] *DELFLY*. www.delfly.nl/.

[9] H. V. Phan, Q. T. Truong and H. C. Park, "Extremely Large Sweep Amplitude Enables High Wing Loading in Giant Hovering Insects," *Bioinspiration & Biomimetics*, vol. 14, no. 6, pp. 066006, 2019, DOI: 10.1088/1748-3190/ab3d55.

[10] H. V. Phan and H. C. Park, "Design and Evaluation of a Deformable Wing Configuration for Economical Hovering Flight of an Insect-like Tailless Flying Robot," *Bioinspiration & Biomimetics*, vol. 13, no. 3, pp. 036009, 2018, DOI: 10.1088/1748-3190/aab313.

[11] Q. T. Truong, et al, "A Modified Blade Element Theory for Estimation of Forces Generated by a Beetle-mimicking Flapping Wing System," *Bioinspiration & Biomimetics*, vol. 6, no. 3, pp. 036008, 2011, DOI: 10.1088/1748-3182/6/3/036008.

[12] Y. Chen, et al, "Controlled Flight of a Microrobot Powered by Soft Artificial Muscles," *Nature*, vol. 575, no. 7782, pp. 324-329, 2019, DOI: 10.1038/s41586-019-1737-7.

[13] J. Forshaw, *Encyclopedia of Birds*. New York. Smithmark, 1991: 496.

[14] H. V. Phan, S. Aurecianus, T. K. Au, T. Kang and H. C. Park, "Towards the Long-Endurance Flight of an Insect-Inspired, Tailless, Two-Winged, Flapping-Wing Flying Robot," *IEEE Robotics and Automation Letters*, vol. 5, no. 4, pp. 5059-5066, 2020 DOI: 10.1109/LRA.2020.3005127.

[15] H. V. Phan, S. Aurecianus, T. Kang and H. C. Park, "KUBeetle-S: An Insect-like, Tailless, Hover-capable Robot That Can Fly with a Low-torque Control Mechanism," *International Journal of Micro Air Vehicles*, vol. 11, pp. 175682931986137, 2019, DOI: 10.1177/1756829319861371.

[16] M. Karásek, "Good Vibrations for Flapping-wing Flyers," *Science Robotics*, vol. 5, no. 46, 2020, DOI: 10.1126/scirobotics.abe4544.

[17] H. V. Phan and H. C. Park, "Insect-inspired, Tailless, Hover-capable Flapping-wing Robots: Recent Progress, Challenges, and Future Directions," *Progress in Aerospace Sciences*, vol. 111, pp. 100573, 2019, DOI: 10.1016/j.paerosci.2019.100573.

[18] D. D. Chin and D. Lentink, "Flapping Wing Aerodynamics: From Insects to Vertebrates," *Journal of Experimental Biology*, vol. 219, no. 7, pp. 920-932, 2016, DOI: 10.1242/jeb.042317.